

# 1 **Gap-Filling of Turbulent Heat Fluxes over Rice–Wheat-Rotation** 2 **Croplands Using the Random Forest Model**

3 Jianbin Zhang<sup>1</sup>, Zexia Duan<sup>1</sup>, Shaohui Zhou<sup>1</sup>, Yubin Li<sup>1</sup>, Zhiqiu Gao<sup>1</sup>

4 <sup>1</sup> School of Atmospheric Physics, Nanjing University of Information Science & Technology, Nanjing, 210044, China

5 *Correspondence to:* Dr. Yubin Li (liyubin@nuist.edu.cn)

6 **Abstract.** This study investigated the accuracy of the Random Forest (RF) model in gap-filling the sensible (H) and latent heat  
7 (LE) fluxes, by using the observation data collected at a site over rice–wheat-rotation croplands in Shouxian County of eastern  
8 China from 15 July 2015 to 24 April 2019. Firstly, the variable significances of the machine learning (ML) model’s five input  
9 variables, including the net radiation (Rn), winds speed (WS), temperature (T), relative humidity (RH), and air pressure (P),  
10 were examined, and it was found that Rn accounted for 78% and 76% of the total variable significance in H and LE calculating,  
11 respectively, showing that it was the most important input variable. Secondly, the RF model’s accuracy with the five-variable  
12 (Rn, WS, T, RH, P) input combination was evaluated, and the results showed that the RF model could reliably gap-fill the H  
13 and LE with mean absolute errors (MAEs) of 5.88 Wm<sup>-2</sup> and 20.97 Wm<sup>-2</sup>, and root mean square errors (RMSEs) of 10.67 Wm<sup>-2</sup>  
14 and 29.46 Wm<sup>-2</sup>, respectively. Thirdly, 4-variable input combinations were tested, and it was found that the best input  
15 combination was (Rn, WS, T, P) by removing RH from the input list, and its MAE values of H and LE were reduced by 12.65%  
16 and 7.12%, respectively. At last, through the Taylor diagram, H and LE gap-filling accuracies of the RF model, the support  
17 vector machine (SVM) model, the k-nearest neighbor (KNN) model, and the gradient boosting decision tree (GBDT) model  
18 were inter-compared, and the statistical metrics showed that RF was the most accurate for both H and LE gap-filling, while  
19 the LR and KNN model performed the worst for H and LE gap-filling, respectively.

20

## 21 **1 Introduction**

22 The turbulent fluxes between the atmosphere and the ground play a crucial role in global climate change and atmospheric  
23 circulation, and the inaccuracy of long-term observations of surface turbulent fluxes is a major factor in erroneous weather  
24 predictions and climate projections. Research on the ecological effects of urban green spaces, agricultural ecosystems, and  
25 forests all use surface turbulent fluxes as key indicators. Currently, the eddy covariance (EC) technique can be used to directly  
26 measure the turbulent fluxes (Wilson et al., 2001; Jiang et al., 2021; Wang et al., 2021). However, due to sensor failure and  
27 adverse meteorological factors (such as rainfall and frost), these high-frequency turbulence data are subject to errors (Khan et  
28 al., 2018). As a result, it is difficult to obtain a continuous time series of ground-based turbulent fluxes. Furthermore, quality  
29 assurance methods lead to unavailable sections of flux datasets (Nisa et al., 2021). Based on the above reasons, gap-filling is  
30 in need to retrieve continuous datasets of EC-based fluxes. Researchers have developed approaches based on existing

31 meteorological information to fill up the gaps in atmospheric databases, such as interpolation, nonlinear regression, mean  
32 diurnal method, and sampling techniques from the marginal distribution (Falge et al., 2001; Hui et al., 2004; Stauch et al.,  
33 2006; Foltnov et al., 2020). Further, the ML technique has also become an effective method to be used in the calculation of  
34 turbulent fluxes (McCandless et al., 2022).

35

36 As a result of recent developments in high computing technology, machine-learning-based algorithms have been developed  
37 and successfully used in various areas, such as natural language processing, data mining, biometrics, computer vision, search  
38 engines, clinical applications, video games, robots, etc. To address the missing data issue, machine-learning-based models  
39 have recently been used to fill data gaps in meteorological elements and turbulent fluxes (Bianco et al., 2019; Yu et al., 2020).  
40 As a result of their reliable and repeatable results, these models are now regarded as a standard gap-filling algorithm (Beringer  
41 et al., 2017; Isaac et al., 2017). ML algorithms have several deficiencies even if they perform well in some areas. For instance,  
42 over-fitting is a major concern that can occur when the training window is too short or the training dataset's quality is poor.  
43 That's because the present ML approaches are not sufficiently adaptable to work in extreme situations with large values  
44 (Kunwor et al., 2017; Moffat et al., 2007). Furthermore, even with the best technique, the model uncertainty of gap-filling still  
45 plays a role, particularly when the gaps are relatively large. Numerous novel ML and optimization algorithms have been created  
46 and put to use in numerous scientific domains since the 2000s, and their superiority has been demonstrated, either singly or as  
47 a component of a hybrid or ensemble model (e.g. Gani et al., 2016).

48

49 Based on the need for fluxes dataset gap-filling, and the effectivity of the ML technique, this paper aims, firstly, to investigate  
50 the performance of the RF machine learning algorithm trained from a dataset obtained over rice-wheat-rotation croplands in  
51 Shouxian County, eastern China, in gap-filling the sensible and latent heat fluxes; and secondly, to analyze the RF model's  
52 accuracy with various meteorological input combinations during training; and thirdly, to compare the performance of RF model  
53 with other four typical ML models.

54

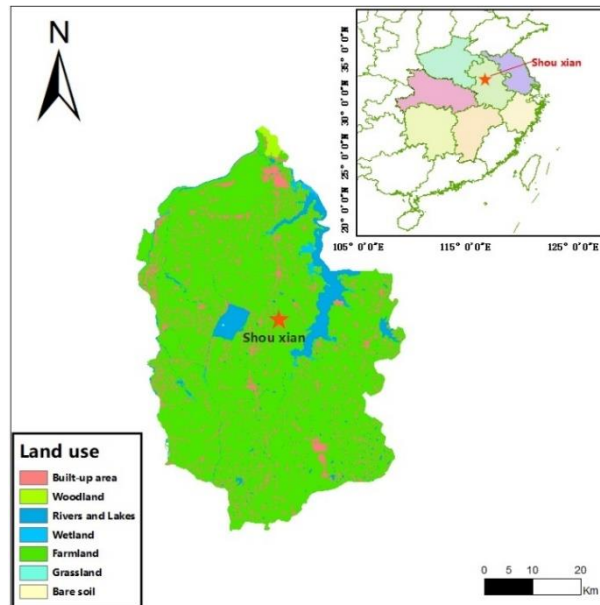
## 55 **2 Materials and Methods**

### 56 **2.1 Study area**

57 This observation was conducted at a site in Shouxian County in the eastern Chinese province of Anhui (32.42 °N, 116.76 °E)  
58 (Figure 1). The altitude of the site is 27 meters, and the annual mean air temperature and annual cumulative precipitation here  
59 are 16 °C and 1115 mm, respectively. Summer (from June to September) precipitation accounts for nearly 60% of the annual  
60 precipitation amount, which meets the high water demand of rice. Drought sometimes occurs due to lack of precipitation in  
61 the growing season of wheat. This observation site is rather flat, with farmland accounting for more than 90% of the area.  
62 Winter wheat is grown here from November until late May, while from June to November the field is flooded, plowed, and

63 harrowed as rice paddies (Duan et al., 2021) (Figure 2). The subtropical northern boundary of the monsoon humid climatic  
 64 type describes the area's climate.

65



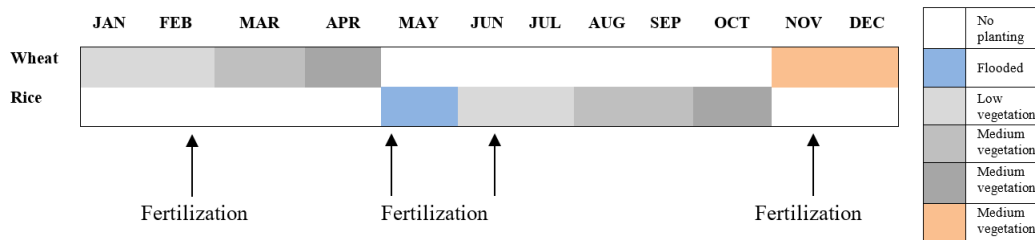
66

67

68

**Figure 1. Geographical location and land-cover map of Shouxian County.**

69



70

71

72

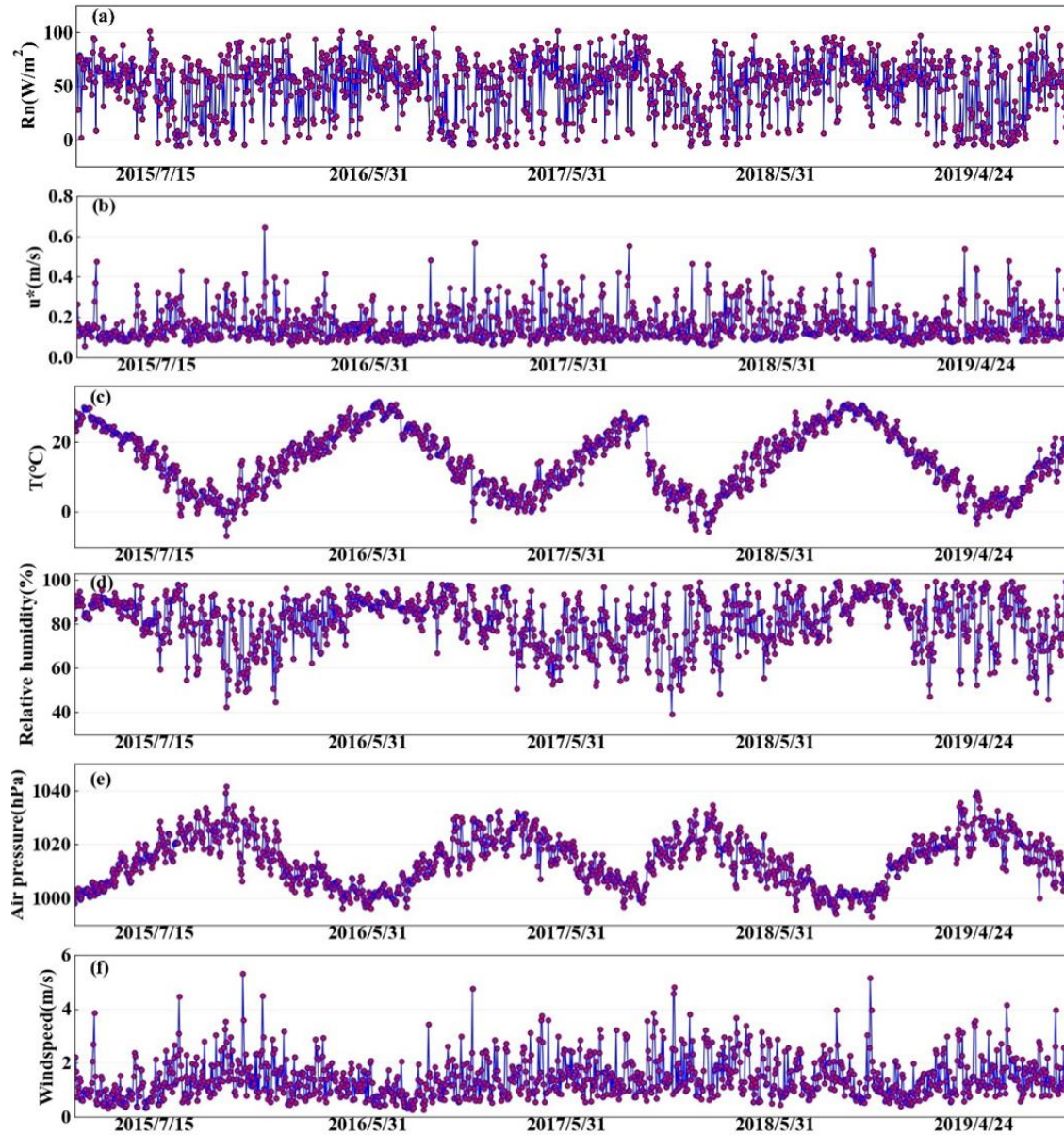
**Figure 2. Crop calendars for the rice and wheat in the North Yangtze River Delta region.**

73

## 74 2.2 Data

75 Over the site described above, EC sensors (EC 150, Campbell Scientific Inc., Logan, UT, USA) were installed at 2.5 meters  
 76 above the ground, including a three-dimensional sonic anemometer (CSAT3, Campbell Scientific Inc., Logan, UT, USA) and  
 77 a CO<sub>2</sub>/H<sub>2</sub>O open-path infrared gas analyzer. The sensible and latent heat fluxes were computed half-hourly using EddyPro

78 software, with time lag compensation, double coordinate rotation, spectrum correction, and Webb-Pearman-Leuning density  
79 correction (Wutzler et al., 2018; Anapalli et al., 2019). Poor-quality fluxes (Eddypro quality check flag value=2) were  
80 discarded. And a quality check based on the relationship between the measured flux and friction velocity was carried out to



81  
82  
83  
84  
85

**Figure 3. Daily averaged a) Rn: net radiation( $Wm^{-2}$ ), b)  $u^*$ : friction velocity(m/s), c) T: air temperature( $^{\circ}C$ ), d) RH: relative humidity(%), e) P: air pressure(hPa), and f) WS:wind speed( $m s^{-1}$ ).**

86 remove the biased data (Papale et al., 2006). Then, using the marginal distribution sampling technique, the flow data were gap-  
87 filled (Reichstein et al., 2005). The time series of air temperature, relative humidity, wind speed, air pressure, friction velocity,  
88 and net radiation were also subjected to quality control. The missing data which need gapfilling are H and LE, with 7205 and  
89 16013 missing, accounting for 12.09% and 26.87% respectively. According to the criteria of  $X(h) < (X - 4\sigma)$  or  $X(h) > (X +$   
90  $4\sigma)$ , where  $X(h)$  indicates the time series of the component,  $X$  is the mean across the averaging interval, and  $\sigma$  is the standard  
91 deviation, noisy data were eliminated (Gao et al., 2003). Data observed from 15 July 2015 to 24 April 2019 are used in this  
92 study, and Figure 3 shows the daily average data of Rn: net radiation( $\text{W m}^{-2}$ ),  $u^*$ : friction velocity(m/s), T: air temperature( $^{\circ}\text{C}$ ),  
93 RH: relative humidity(%), P: air pressure(hPa), and WS: wind speed( $\text{m s}^{-1}$ ).  
94

### 95 2.3 The RF Model

96 RF is a machine learning method that is quick, adaptable, and frequently used to analyze classification and regression jobs  
97 (Breiman, 2001). This model can successfully evaluate highly dimensional and multicollinear data and is resistant to overfitting  
98 (Belgiu et al., 2016). The RF model provides a feature-selection tool to assist in determining the importance of the predictor.  
99 The contribution of each variable to the model, with important variables having a higher effect on the results of the model  
100 evaluation, is the definition of feature significance (Liu et al., 2021). 90% of the data collected at the Shouxian observation  
101 site throughout the study period were used to train the RF model, while the remaining 10% was used to independently validate  
102 the model (hereafter, validation dataset). To lessen the overfitting in this case, a 10-fold cross-validation (CV) procedure was  
103 used (Cai et al., 2020). All training data used here was randomly divided into ten subsamples of equal size for the 10-fold CV  
104 tests. And nine out of the ten subsamples were used as training data (hereafter, training dataset), while the remaining subsample  
105 was used as testing data (hereafter, testing dataset). All ten of the subsamples were utilized as testing data exactly once for  
106 each of the 10 iterations of the CV procedure. One estimate was created by averaging the 10 findings from the folds. We  
107 modified the four RF model hyperparameters based on Bayesian optimization to get the optimal model (Baareh et al., 2021;  
108 Frazier, P.I., 2018): the maximum number of features considered to split a node (Max features), the maximum number of trees  
109 to build (n estimators), the minimum sample number placed in a node prior to the node being split (min split), and the maximum  
110 number of levels for each decision tree (Max depth). Bayesian optimizer is used to tune parameters, you can quickly find an  
111 acceptable hyperparameter value, compared with grid search, the advantage is that the number of iterations is less (time saving),  
112 the granularity can be very small. For example, if we want to adjust the regularized hyperparameters of linear regression, we  
113 set the black box function to linear regression, the independent variable is a hyperparameter, the dependent variable is linear  
114 regression in the training set accuracy, set an acceptable black box function dependent variable value, such as 0.95, the obtained  
115 hyperparameter result is a hyperparameter that can make the linear regression accuracy exceed 0.95. The simulated  
116 performance of the 10-fold CV outcomes was evaluated using four statistical metrics: the correlation coefficient ( $r$ ), mean  
117 absolute error (MAE), root mean square error (RMSE), and standard deviation( $\sigma_n$ ). As a result, the final RF model's parameters  
118 were adjusted to n estimators = 246, min split = 2, Max features = 10, and Max depth = 35, to have the best statistical metrics.

119 The four statistical metrics are calculated by:

$$120 \quad r = \frac{\sum_{i=1}^N (S_i - \bar{S})(O_i - \bar{O})}{\sqrt{\sum_{i=1}^N (S_i - \bar{S})^2} \sqrt{\sum_{i=1}^N (O_i - \bar{O})^2}}, \quad (1)$$

121

$$122 \quad \text{MAE} = \frac{1}{N} \sum_{i=1}^N |S_i - O_i|, \quad (2)$$

123

$$124 \quad \text{RMSE} = \sqrt{\frac{\sum_{i=1}^N (S_i - O_i)^2}{N}}, \quad (3)$$

125

$$126 \quad \sigma_n = \sqrt{\frac{\sum_{i=1}^N (S_i - O_i)^2}{N}}. \quad (4)$$

127

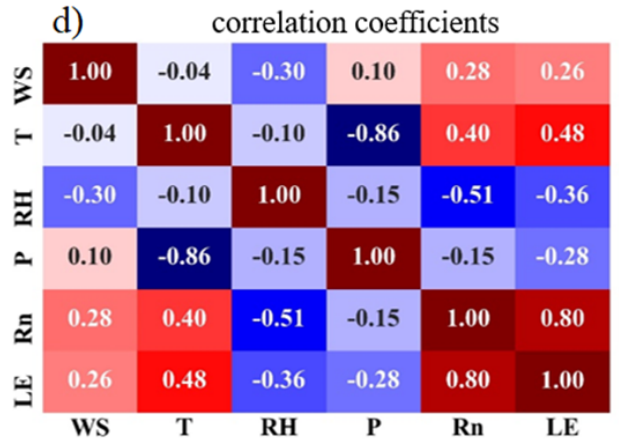
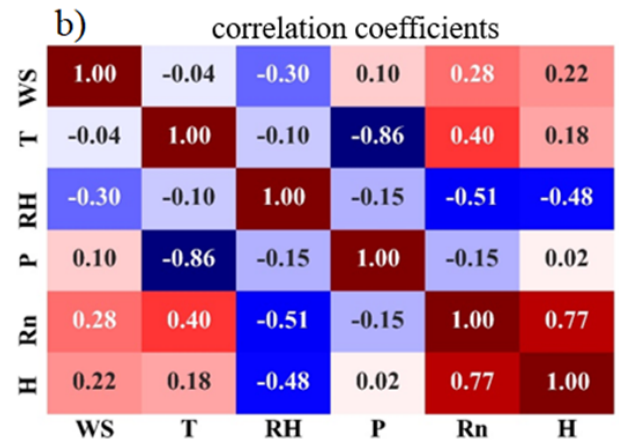
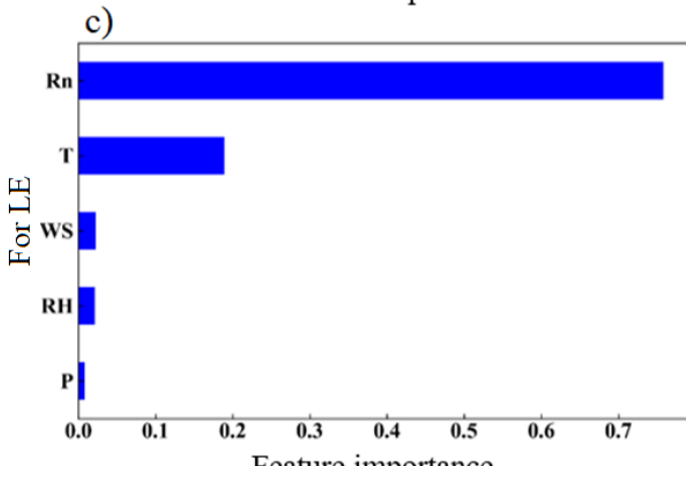
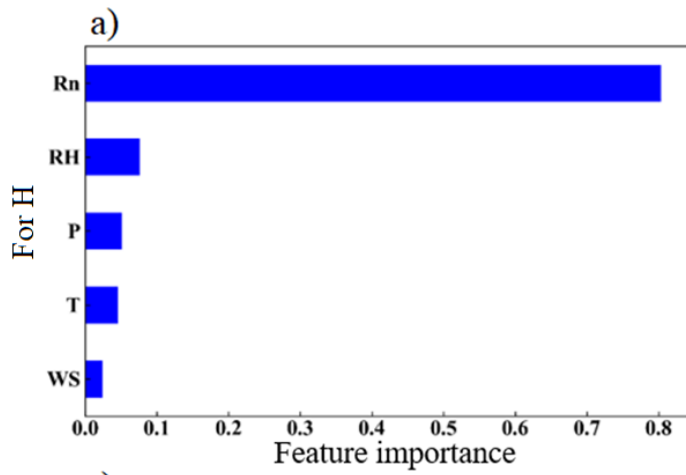
128 where  $S$  stands for the modeled value,  $O$  is the observation,  $\bar{O}$  is the mean observed value, and  $\bar{S}$  is the mean modeled  
129 observation,  $\sigma_n$  indicates the standard deviation. The subscript  $i$  represents the serial number of samples, and  $N$  represents the  
130 total number of samples.

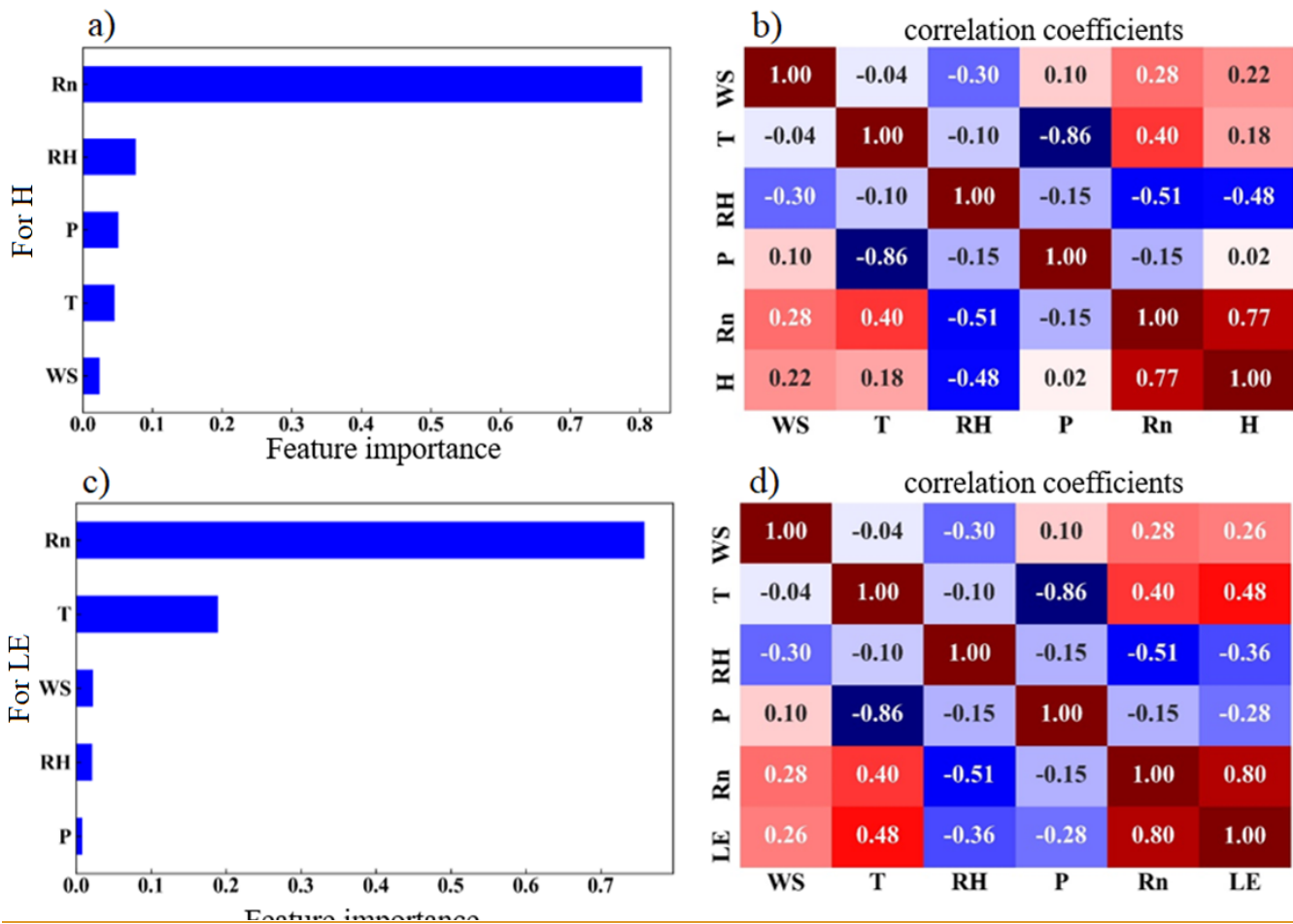
131

## 132 3 Results and discussion

### 133 3.1 Driving Factors of H and LE on a Seasonal Scale

134 The possible driving factors of H and LE were investigated to determine their respective contributions by the RF model as  
135 shown in Figure 4. Rn, which accounted for 78% and 76% of the total variable significance of H and LE, respectively, was the  
136 most crucial variable in regulating the heat fluxes (Figures 4a and 4c). Consistent with the high variable significance values,  
137 H and LE also had the highest  $r$  of 0.79 and 0.75 with H and LE, respectively, as shown in Figures 4b and 4d. The other four  
138 factors contributed much smaller than Rn, and WS, T, RH, and P had importance values of 2%, 4%, 7%, and 5% (2.2%, 19%,  
139 2%, and 0.6%) for H (LE), respectively. All these elements such as Rn, T, WS, RH are normalized before the model starts  
140 training. When these elements are normalized, it ensures uniformity and comparability. In general, all of these predictors  
141 played a role in the H and LE calculation, and for H, the sequence of importance was Rn, RH, P, T, and WS; while for LE, it  
142 was Rn, T, WS, RH, and P. The most significant impact on the change of H and LE came from Rn, which was the most  
143 important energy source of the surface and modulated the surface temperature directly. RH and T had a minor impact on the  
144 H and LE changes in terms of climatic parameters, which carried the information of the light-dependent reactions of H and LE  
145 fluxes. Particularly, WS and P had the minimal impacts on the H and LE fluxes. The WS, T, and RH also affected H and LE  
146 according to the Monin-Obukhov similarity theory (Monin and Obukhov, 1954), while P represented the contributions from  
147 the background weather systems.





149

150  
151  
152

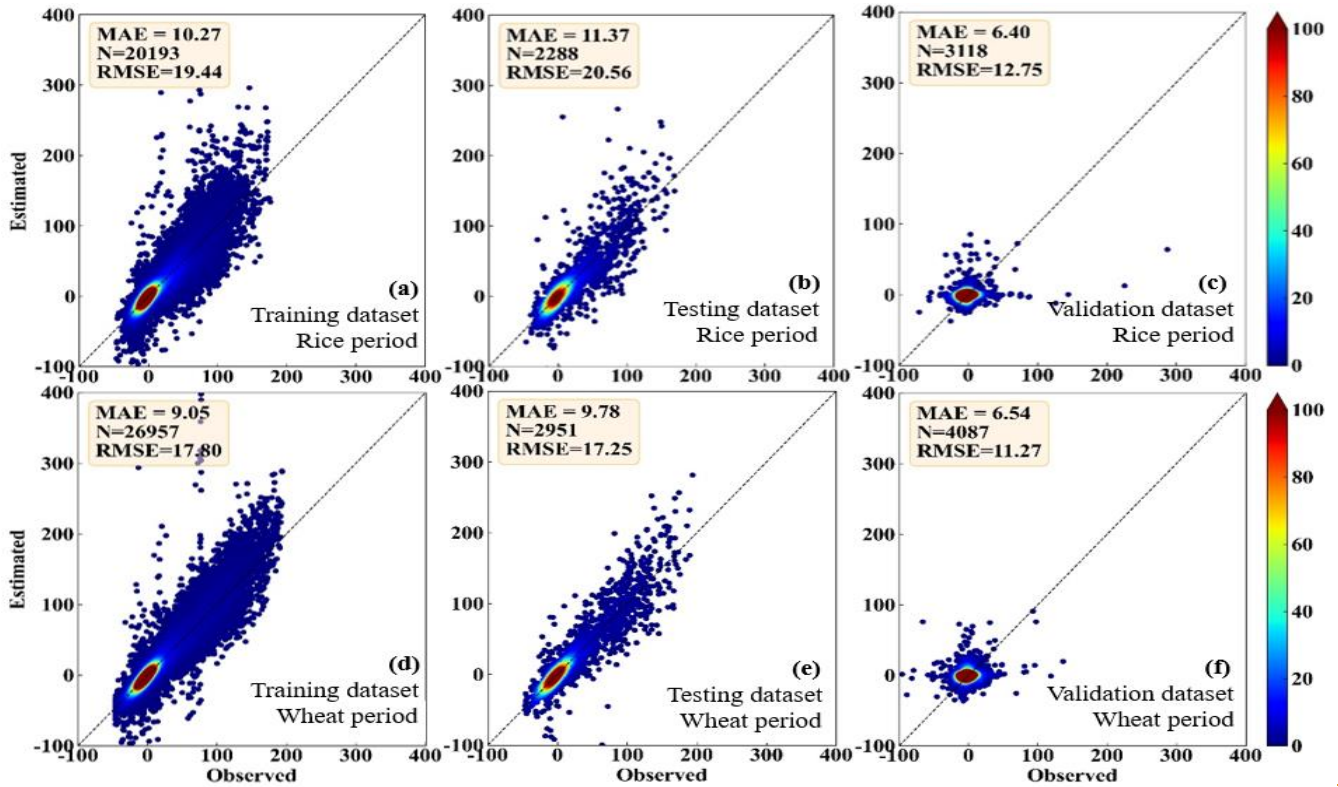
Figure 4. The feature importance of the variables for a) H and c) LE, and the correlation coefficient between each of the input variables for b) H and d) LE.

153 **3.2 RF Model Evaluation**

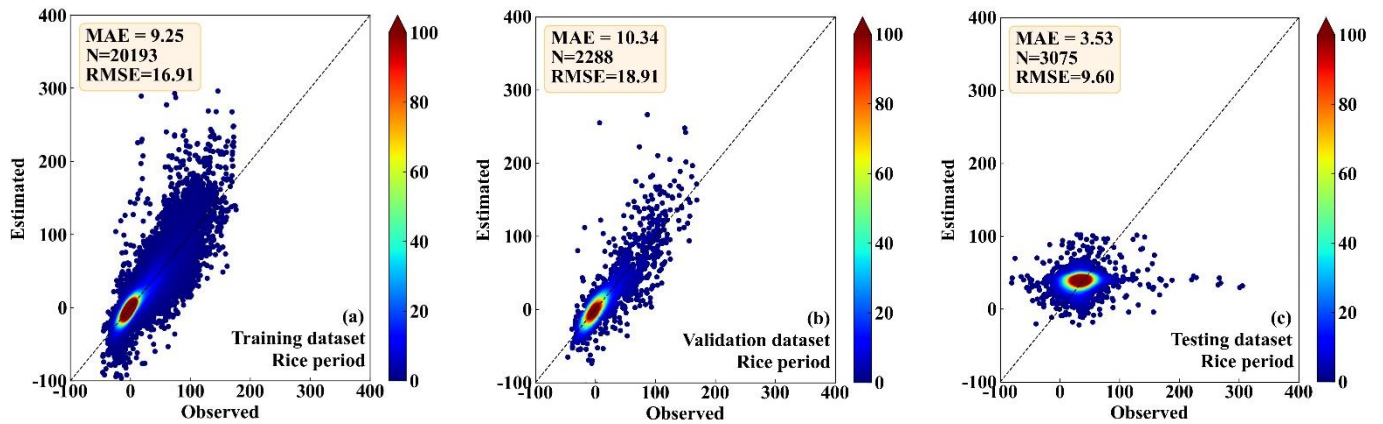
154 Figures 5-6 show the comparison between the observed and the RF-estimated H and LE, respectively. In the period of rice, the  
 155 RF model showed good performance for both the training dataset (MAE=8.51 and 17.89 Wm<sup>-2</sup>; RMSE =14.11 and 29.82 Wm<sup>-2</sup>,  
 156 for H and LE, respectively) and the testing dataset (MAE =9.61 and 10.34 Wm<sup>-2</sup>, RMSE = 15.63 and 17.21Wm<sup>-2</sup>, for H and  
 157 LE, respectively) (Figures 5a, 5b, 6a, and 6b). RF model also showed high consistency with direct measurements for the  
 158 validation dataset (MAE=5.88 and 20.97 Wm<sup>-2</sup>, RMSE = 10.67 and 29.46 Wm<sup>-2</sup>, for H and LE, respectively), (Figures 5c and  
 159 6c). In the period of wheat, the performance of the RF model for the training, testing, and validation datasets of H and LE was  
 160 similar to that in the period of rice. For the training, testing, and validation datasets, respectively, the MAEs are 7.18, 8.01,  
 161 and 6.01 Wm<sup>-2</sup> for H, and 13.58, 8.82, and 19.93 Wm<sup>-2</sup> for LE; and the RMSEs are 12.27, 13.61, and 9.86 Wm<sup>-2</sup> for H, and

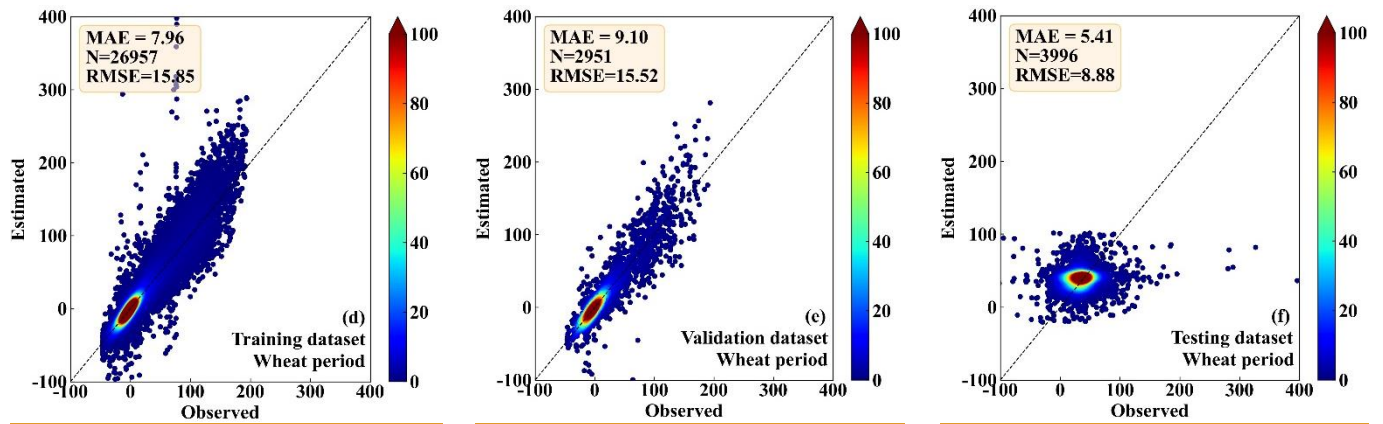


162 24.92, 15.17, and 28.74  $\text{Wm}^{-2}$  for LE (Figure 5d,e,f, Figure 6 d,e,f). These results demonstrate that the RF model is capable of  
163 effectively calculating the H and LE with input variables of Rn, WS, T, RH, and P.



164  
165

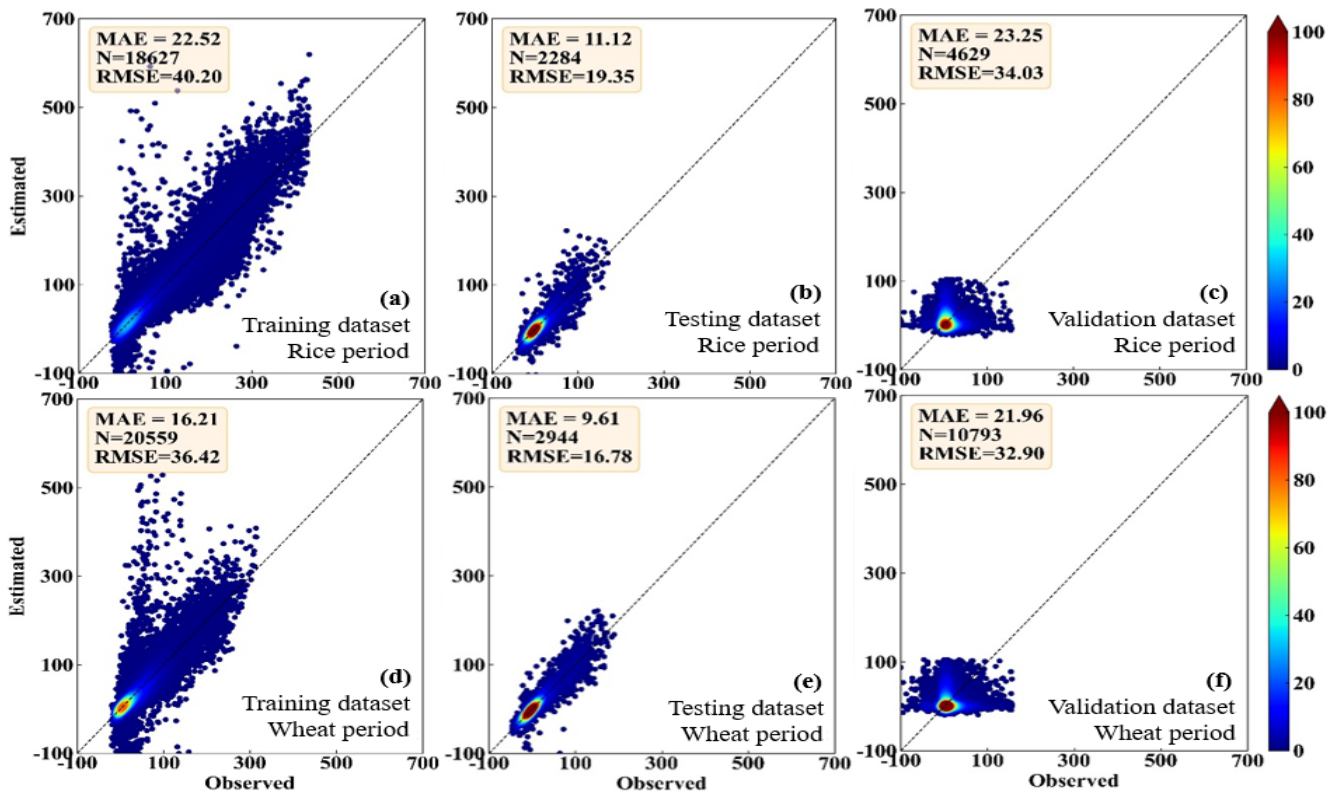




166

167 **Figure 5.** Scatter density plots of the observed and the RF-estimated H values, a) and d) for the training dataset, b) and e) for the  
 168 **testing/validation** dataset, and c) and f) for the **validation/testing** dataset. And a), b) and c) are in the period of rice, while d), e) and  
 169 f) are in the period of wheat.

170



171

172

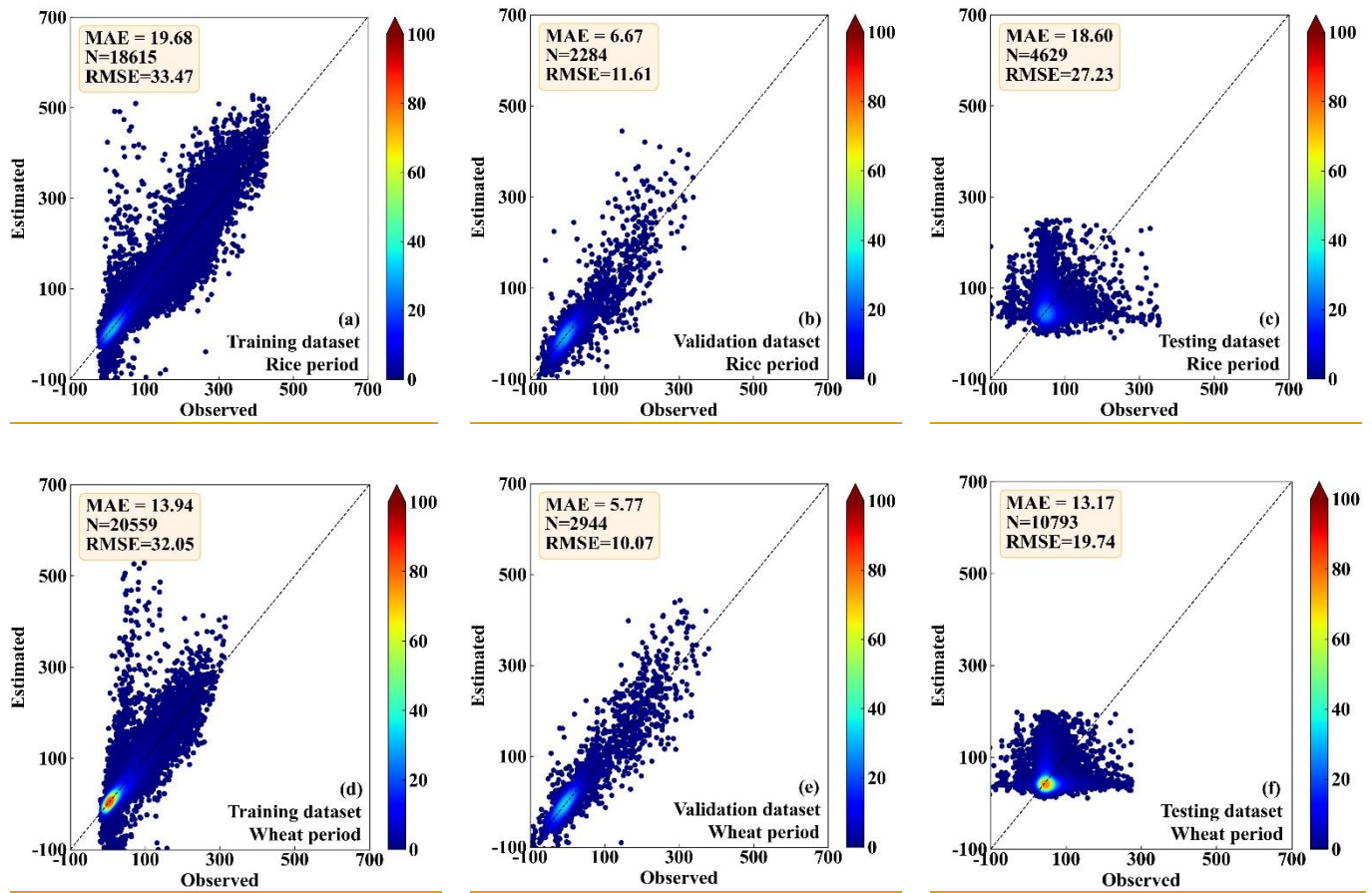


Figure 6. Same as Figure 5, but for LE.

173

174

### 175 3.3 Examination of Input Combinations

176 Meteorological elements may occasionally be unavailable due to the failure of sensors so the 5-variable input combination  
 177 derived in Section 3.2 is not always applicable. Therefore, examination of other alternative input combinations is important to  
 178 have substitute choices for data gap-filling when the 5-variable input combination is unavailable. In this subsection, we  
 179 investigated the RF model's performance under the situation of lacking one element in the 5-variable input combination, i.e.,  
 180 we tested the 4-variable input combinations of (WS, T, RH, P), (Rn, T, RH, P), (Rn, WS, RH, P), (Rn, WS, T, P), and (Rn,  
 181 WS, T, RH), by removing Rn, WS, T, RH, and P from the 5-variable input combination, respectively. The MAEs and RMSEs  
 182 for these combinations are shown in Table 1, and it demonstrates that the RF model's accuracy may either increase or decrease  
 183 as a result of the removal of a meteorological element during the training phase. For instance, it was found that the model's  
 184 performance greatly improved once RH was eliminated from the input combination, with the MAE and RMSE of H decreasing

185 from 6.48 and 11.94  $\text{Wm}^{-2}$  to 5.66 and 11.06  $\text{Wm}^{-2}$ , respectively, and LE from 19.1 and 39.39  $\text{Wm}^{-2}$  to 17.74 and 35.27  $\text{Wm}^{-2}$ .  
186 <sup>2</sup>. This outcome is logical given that RH and H do not have a strong correlation, as a result, performance will be enhanced if  
187 RH is not included in the gap-filling processing pipeline. According to our findings, the RF model's performance may be  
188 greatly enhanced by excluding irrelevant meteorological elements from the study and choosing only those that have a  
189 significant impact on the variable. Our findings imply that in order to attain the best gap-filling accuracy, it is necessary to  
190 take into account both the advantages and disadvantages of ML-based models as well as the ideal input components.The results  
191 suggested that RH at a single level was not well correlated to the fluxes as shown in Section 3.1, because the one-level RH  
192 was strongly affected by the irrigation activity which was an external factor of the weather system. As a result, RF model  
193 performance was enhanced when the irrelevant variable (i.e., RH) was removed from the input list. The same condition also  
194 happened to the removal of WS, as could be seen from Section 3.1, WS showed small correlations with the fluxes. WS over  
195 this site was rather small, and frequently below  $2 \text{ m s}^{-1}$ , and under this light wind condition, the fluxes were mostly driven by  
196 the buoyancy rather than the wind shear. Figure 7 presents the MAE variation percentage of the 4-variable input combinations  
197 from the 5-variable input combination. After RH was removed from the input list, the RF model showed favorable performance  
198 for both H and LE, as shown in Figure 7, with MAE values improvements of 12.65 and 7.12%, respectively. Notably, the  
199 removal of Rn from the input combination resulted in a considerable decline in the RF model's performances, with MAE  
200 degradation percentage values reaching 16.20% and 10.73%, respectively. This outcome makes sense since Rn is highly  
201 associated with H and LE; hence, performance will be declined if Rn is left out of the input training dataset. As a consequence,  
202 our findings demonstrated that choosing strongly associated components could greatly increase the gap-filling accuracy.  
203 According to our findings, the best input combination is (Rn, WS, T, P).

204

205 **Table 1. The MAEs and RMSEs of the RF-estimated heat fluxes for the 4-variable input combinations, and the corresponding**  
206 **changes from the 5-variable input combination.**

207

Factors Included	Factors Eliminated		MAE (change)	RMSE (change)
<b>WS, T, RH, P</b>	Rn	H	7.63 (+1.15)	10.72 (-1.22)
		LE	21.15 (+2.05)	39.38 (-4.62)
<b>Rn, T, RH, P</b>	WS	H	6.15 (-0.33)	11.42 (-0.52)
		LE	18.36 (-0.74)	36.13 (-2.34)
<b>Rn, WS, RH, P</b>	T	H	6.68 (+0.20)	11.48 (-0.46)
		LE	19.54 (+0.44)	38.54 (-1.46)
<b>Rn, WS, T, P</b>	RH	H	5.66 (-0.82)	11.06 (-0.88)
		LE	17.74 (-1.36)	35.27 (-4.12)
<b>Rn, WS, T, RH</b>	P	H	6.49 (+0.03)	11.77 (-0.17)
		LE	19.12 (+0.02)	38.13 (-1.07)

208

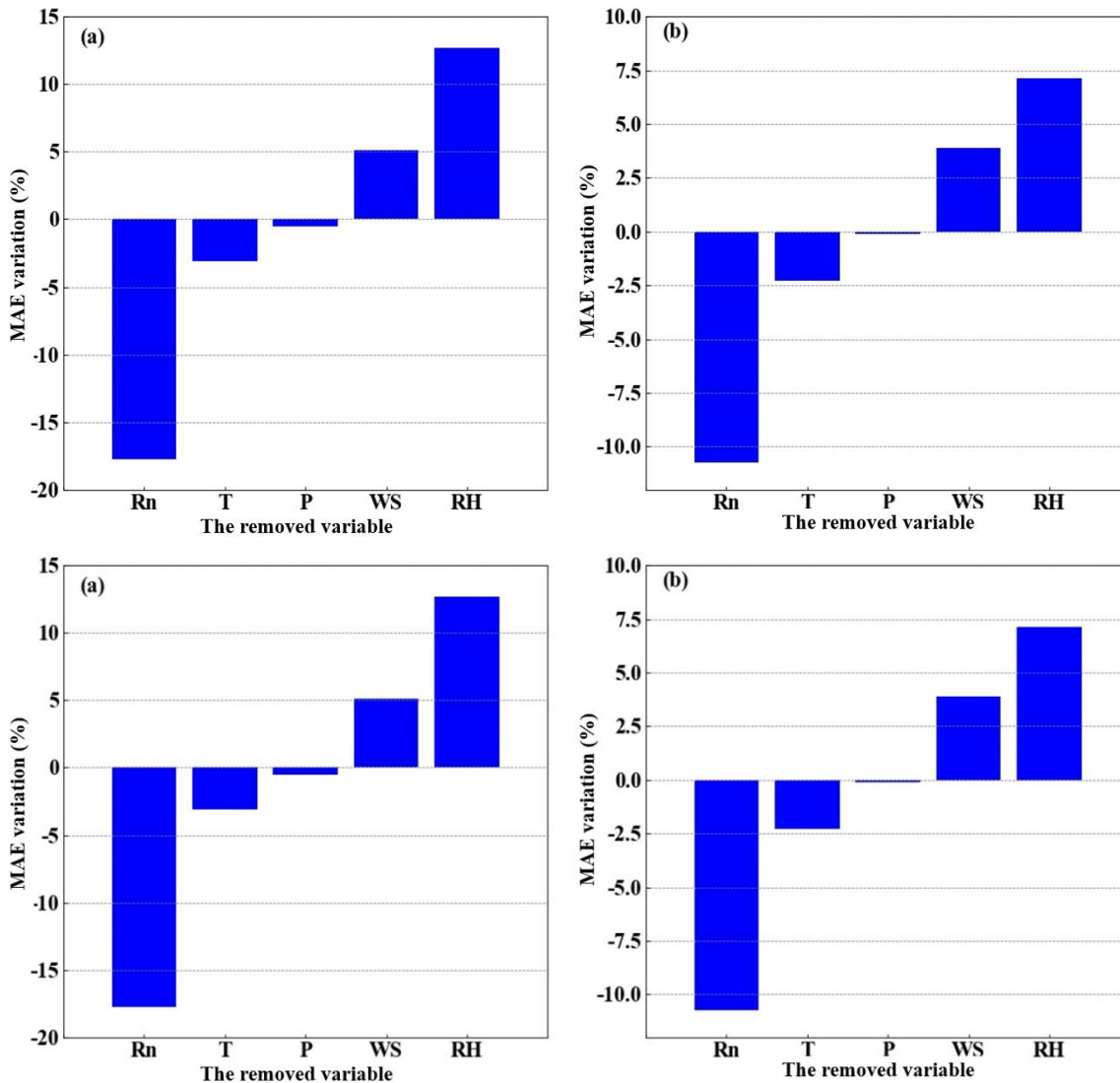


Figure 7. The MAE percentage variation after changing the 5-variable input combinations to the 4-variable input combinations, a) for H, and b) for LE, respectively. The x-axis labels indicate the removed variables.

It should be noted that other variables that might have an impact on the H and LE were not investigated here. For example, given that our research site was over farmland and plants were growing, knowledge of the variations of the leaf area index (LAI) and inclusion of it to the training dataset should also be useful to increase the accuracy of the RF model in H and LE gap-filling. The monsoonal climate here also incurred considerable precipitation variations, which might as well potentially contribute to the RF model accuracy improvement. However, due to the lack of LAI and precipitation observations, the inclusion of the two variables into the RF model training dataset was not applicable in this study. Additionally, as shown above,

221 more variables would bring a higher observation demand, and lead to more complexity and potentially decreased results, such  
222 as the adding variable of RH.

223

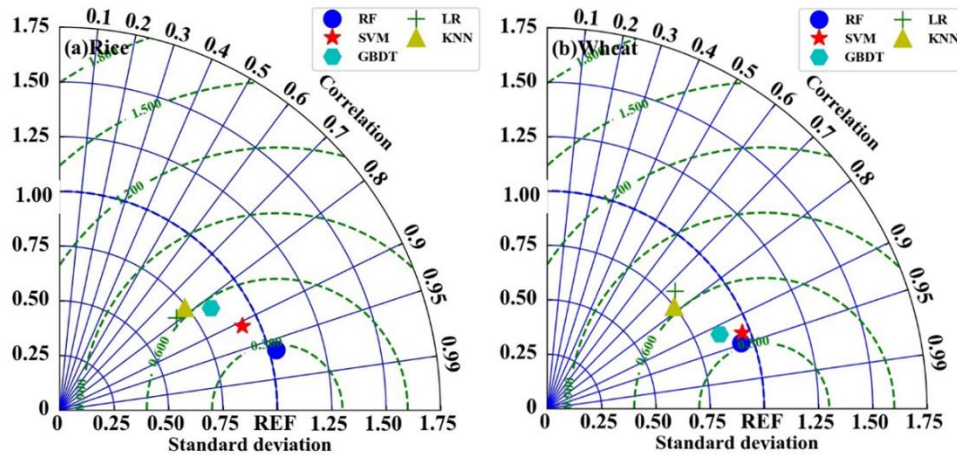
### 224 3.4 Comparison with other four ML methods

#### 225 3.4.1 Comparison in H estimation

226

227 To further investigate the reliability of the RF model, we used a Taylor diagram to compare its performance in H estimation  
228 with other four ML models: ~~linear regression (LR), k-nearest neighbor (KNN), support vector machine (SVM), and gradient~~  
229 ~~boosting decision tree (GBDT).~~ support vector machine (SVM), k-nearest neighbor (KNN), gradient boosting decision tree  
230 (GBDT), and linear regression (LR). SVM is a data-oriented classification algorithm, and the basic model is to find the best  
231 separation hyperplane on the feature space so that the positive and negative sample intervals on the training set are maximum.  
232 Its advantages are that the kernel function can be used to map to a high-dimensional space; the use of the kernel function can  
233 solve the nonlinear classification ; the classification idea is very simple, that is, to maximize the interval between the sample  
234 and the decision-making surface ;the classification effect is better ;and the nonlinear relationship between data and features is  
235 easy to obtain when the small and medium-sized sample size is large.KNN is particularly suitable for multi-classification  
236 problems. Its advantage is that it is simple in thought, easy to understand, easy to implement; No estimation parameters, no  
237 training; High accuracy, insensitive to outliers.GBDT can flexibly handle various types of data, including continuous and  
238 discrete values. With relatively few parameter adjustment times, the prediction preparation rate can also be relatively high. If  
239 the data dimension is high, the computational complexity of the algorithm will increase. Using some robust loss functions, the  
240 robustness to outliers is very strong.LR is a statistical analysis method that uses regression analysis in mathematical statistics  
241 to determine the quantitative relationship between two or more variables that depend on each other.The results have good  
242 interpretability, can intuitively express the importance of each attribute in the prediction, and the calculation of entropy is not  
243 complicated.

244 All the models were optimized with the same technique described above for the RF model. The results are shown in Figure 8.  
245 The EC measurements were used as the benchmark. It can be seen that the RF model generally outperforms the other four  
246 models, with the standard deviations ( $\sigma_n$ ) and correlation values of 1.05 and 0.98 during the period of rice planting, and 0.96  
247 and 0.95 during the period of wheat planting, respectively. The SVM model is the second most accurate model, with the  $\sigma_n$  and  
248 correlation of 0.92 and 0.98 during the period of rice planting, and 0.91 and 0.93 during the period of wheat planting,  
249 respectively. The LR model performs the worst, with the  $\sigma_n$  and correlation of 0.60 and 0.76 during the period of rice planting,  
250 and 0.80 and 0.72 during the period of wheat planting, respectively. The accuracy of KNN and the GBDT models is in between  
251 the above-discussed models, and the  $\sigma_n$  and correlation during the rice and wheat period for KNN are 0.68 and 0.73, and 0.77  
252 and 0.82; and for GBDT are 0.79 and 0.80, and 0.81 and 0.9, respectively.



254

255

256

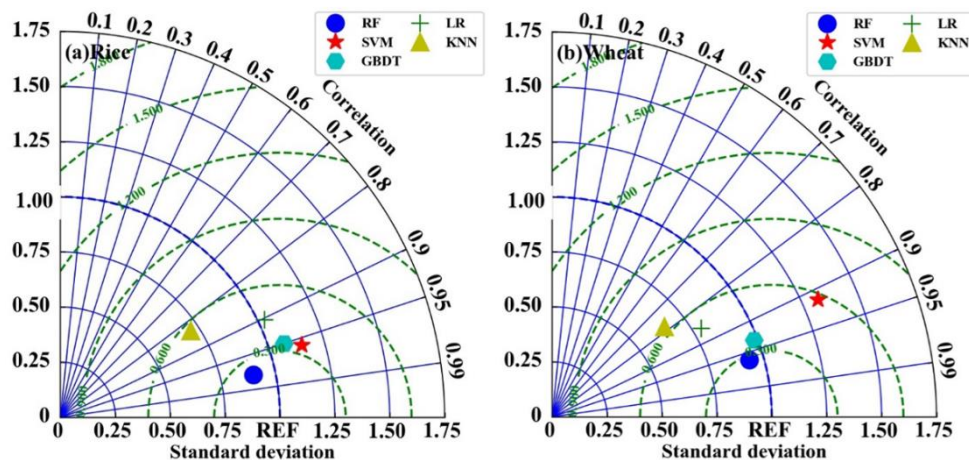
Figure 8. The performances of the five models for estimating H in the period of a) rice and b) wheat.

257

### 258 3.4.2 Comparison in LE estimation

259

260 Figure 9 illustrates a comparison of the estimated LE by all five models during the period of rice and wheat planting. The  
 261 results are similar to those in the H estimation, and the RF model is found to perform better than the other four models, with  
 262 the  $\sigma_n$  and correlation values of 0.95 and 0.97 during the period of rice planting, and 0.97 and 0.96 during the period of wheat  
 263 planting, respectively. Nonetheless, the KNN model performs the worse for LE estimating and has the  $\sigma_n$  and correlation  
 264 values of 0.68 and 0.82 during the period of rice planting, and 0.62 and 0.79 during the period of wheat planting, respectively.  
 265 Overall, as shown by the Taylor diagram of Figures 8 and 9, in this study the RF model has the best accuracy in either H or  
 266 LE estimation for data gap-filling.



267

268  
269  
270

**Figure 9. Same as Figure 8, but for LE**

#### 271 **4 Summary and Conclusions**

272 To assess the RF model's capacity for gap-filling the sensible and latent heat flux measurements over rice-wheat rotation  
273 croplands, 90% of the total observation data gathered at Shouxian were utilized for training and testing, and the remaining 10%  
274 for independent validation. Our findings demonstrate that Rn is the most important variable in regulating H and LE, and it  
275 accounts for 78% and 76% of the total variable significance in the RF model construction for H and LE calculation, respectively.  
276 The least important variables are WS and P, and their total variable significances are 2% and 0.6%, respectively. During the  
277 periods of rice and wheat planting, the RF model with a 5-variable input combination shows reliable performance, with MAE  
278 values of 5.88 Wm<sup>-2</sup> and 20.97 Wm<sup>-2</sup>, and RMSE values of 10.67 Wm<sup>-2</sup> and 29.46 Wm<sup>-2</sup>, respectively. However, further  
279 analysis of the RF model with 4-variable input combinations indicates that the performance of the model is improved when  
280 RH is removed from the input list, and the MAE values decrease by 12.65% and 7.12% for H and LE, respectively. Nonetheless,  
281 the 4- variable input combination without Rn causes an increase in the MAE values of the model, by 16.20% and 10.73% for  
282 H and LE, respectively. Therefore, the best input combination found in this study for heat fluxes gap-filling is (Rn, WS, T, P).  
283 Statistical comparison of RF and other four typical ML models (LR, KNN, SVN, and GBDT) by Tylar diagram further shows  
284 that RF is the most accurate, with the standard deviations and correlation values of 0.95 and 0.97 during the period of rice  
285 planting, and 0.97 and 0.96 during the period of wheat planting, respectively. While the LR and KNN models perform the  
286 worst for H and LE gap-filling, respectively, according to the statistical metrics of the Tylor diagram.

287

288 This study is based on only the data collected over rice–wheat-rotation croplands, but the method presented above to find a  
289 reliable gap-filling ML model can also be used over other types of the underlying surface and in other climate zones. It should  
290 be noted that over different types of the underlying surface and climates, the variable significances can vary and a careful  
291 check of the input combinations is needed. For example, over polar oceans with strong winds, Rn probably is not the most  
292 important driving factor, while the winds which cause mostly the turbulence may take the first place. On the other hand, over  
293 areas without human irrigation activity, RH will possibly be strongly related to the latent heat flux, and hence the inclusion of  
294 it into the input list may increase the ML model performance. Besides the examination of the input combinations, the choice  
295 of an ML model and the method to optimize its parameters are also important.

296

297 Overall, this study shows the potential to use the RF model to produce trustworthy gap-filling data of H and LE over rice–  
298 wheat-rotation croplands, and the ML methods are suggested to be used to derive the fluxes' estimations when direct EC  
299 observations are not available.



301 **References**

- 302 Alavi, N., Warland, J.S., Berg, A.A.: Filling gaps in evapotranspiration measurements for water budget studies: Evaluation of  
303 a Kalman filtering approach, *J. Agric. For. Meteorol.*, 141 (1), 57–66, <https://doi.org/10.1016/j.agrformet.2006.09.011>,  
304 2006.
- 305 Anapalli, S.S.; Fisher, D.K.; Reddy, K.N.; Krutz, J.L.; Pinnamaneni, S.R.; Sui, R.: Quantifying water and CO<sub>2</sub> fluxes and water  
306 use efficiencies across irrigated C3 and C4 crops in a humid climate, *J. Sci. Total Environ.*, 663, 338–350,  
307 <https://doi.org/10.1016/j.scitotenv.2018.12.471>, 2018.
- 308 Baareh, A.K.; Elsayad, A.; Al-Dhaifallah, M.: Recognition of splice-junction genetic sequences using random forest and  
309 Bayesian optimization, *J. Multimed. Tools Appl.*, 80, 30505–30522, <https://doi.org/10.1007/s11042-021-10944-7>, 2021.
- 310 Belgiu, M.; Dragut, L.: Random forest in remote sensing: A review of applications and future directions, *Isprs J. Photogramm.*  
311 *J.Remote Sensing.*, 114, 24–31, <https://doi.org/10.1016/j.isprsjprs.2016.01.011>, 2016.
- 312 Beringer, J., McHugh, I., Hutley, L. B., Isaac, P., and Kljun, N.: Technical note: Dynamic INtegrated Gap-filling and  
313 partitioning for OzFlux (DINGO), *J. Biogeosciences.*, 14, 1457–1460, <https://doi.org/10.5194/bg-14-1457-2017>, 2017.
- 314 Best, M. J., M. Pryor, D. B. Clark, G. G. Rooney, et al.: The Joint UK Land Environment Simulator (JULES), model description  
315 - Part 1: Energy and water fluxes, *J. Geosci. Model Dev.*, 4, 677-699, <https://doi.org/10.5194/gmd-4-677-2011>, 2011.
- 316 Bianco, M.J.; Gerstoft, P.; Traer, J.; Ozanich, E.; Roch, M.A.; Gannot, S.; Deledalle, C.-A.: Machine learning in acoustics:  
317 Theory and applications, *J. Acoust. Soc. Am.*, 146, 3590–3628, <https://doi.org/10.1121/1.5133944>, 2019.
- 318 Breiman, L.: Random Forests, *J. Mach. Learn.*, 45, 5–32, <https://doi.org/10.1023/A:1010933404324>, 2001.
- 319 Cai, J.C.; Xu, K.; Zhu, Y.H.; Hu, F.; Li, L.H.: Prediction and analysis of net ecosystem carbon exchange based on gradient  
320 boosting regression and random forest, *J. Appl. Energy.*, 262, 114566, <https://doi.org/10.1016/j.apenergy.2020.114566>,  
321 2020.
- 322 Duan, Z.; Grimmond, C.; Gao, C.Y.; Sun, T.; Liu, C.; Wang, L.; Li, Y.; Gao, Z.: Seasonal and interannual variations in the  
323 surface energy fluxes of a rice–wheat rotation in Eastern China, *J. Appl. Meteorol. Climatol.*, 60, 877–891,  
324 <https://doi.org/10.1175/JAMC-D-20-0233.1>, 2021.
- 325 Duan, Z.; Yang, Y.; Wang, L.; Liu, C.; Fan, S.; Chen, C.; Tong, Y.; Lin, X.; Gao, Z.: Temporal characteristics of carbon  
326 dioxide and ozone over a rural-cropland area in the Yangtze River Delta of eastern China, *J. Sci. Total Environ.*, 757,  
327 e143750, <https://doi.org/10.1016/j.scitotenv.2020.143750>, 2021.
- 328 Falge, E.; Baldocchi, D.; Olson, R.; Anthoni, P.; Aubinet, M.; Bernhofer, C.; Burba, G.; Ceulemans, R.; Clement, R.; Dolman,  
329 H.: Gap filling strategies for defensible annual sums of net ecosystem exchange, *J. Agric. For. Meteorol.*, 107, 43–69,  
330 [https://doi.org/10.1016/S0168-1923\(00\)00225-2](https://doi.org/10.1016/S0168-1923(00)00225-2), 2001.

331 Foltýnov á L.; Fischer, M.; McGloin, R.P.: Recommendations for gap-filling eddy covariance latent heat flux measurements  
332 using marginal distribution sampling, *J. Theor. Appl. Climatol.*, 139, 677–688, [https://doi.org/10.1007/s00704-019-](https://doi.org/10.1007/s00704-019-02975-w)  
333 02975-w, 2020.

334 Frazier, P.I.: A Tutorial on Bayesian Optimization, arXiv 2018, <https://doi.org/10.48550/arXiv.1807.02811>, 2018.

335 Gao, Z. Q., L. G. Bian, and X. J. Zhou.: Measurements of turbulent transfer in the near-surface layer over a rice paddy in China,  
336 *J. Geophys. Res.*, 108(D13), 4387–4387, <https://doi.org/10.1029/2002JD002779>, 2003.

337 Garratt, J. R.: The atmospheric boundary layer. Cambridge Atmospheric and Space Science Series, Cambridge University  
338 Press, 316, <https://doi.org/10.1017/CBO9781316117422>, 2015.

339 Hui, D.; Wan, S.; Su, B.; Katul, G.; Monson, R.; Luo, Y.: Gap-filling missing data in eddy covariance measurements using  
340 multiple imputation (MI) for annual estimations, *J. Agric. For. Meteorol.*, 121, 93–111, [https://doi.org/10.1016/S0168-](https://doi.org/10.1016/S0168-1923(03)00158-8)  
341 1923(03)00158-8, 2004.

342 Isaac, P., Cleverly, J., McHugh, I., Van Gorsel, E., Ewenz, C., and Beringer, J.: OzFlux data: Network integration from  
343 collection to curation, *J. Biogeosciences*, 14, 2903–2928, <https://doi.org/10.5194/bg-14-2903-2017>, 2017.

344 Jiang, L.; Zhang, B.; Han, S.; Chen, H.; Wei, Z.: Upscaling evapotranspiration from the instantaneous to the daily time scale:  
345 Assessing six methods including an optimized coefficient based on worldwide eddy covariance flux network, *J. Hydrol.*,  
346 596, 126135, <https://doi.org/10.1016/j.jhydrol.2021.126135>, 2021.

347 Kepert, J.: Choosing a boundary layer parameterization for tropical cyclone modelling, *J. Mon. Wea. Rev.* [serial online].,  
348 140(5), 1427-1445, DOI: <https://doi.org/10.1175/MWR-D-11-00217.1>, 2012.

349 Khan, M.S.; Jeon, S.B.; Jeong, M.H.: Gap-Filling Eddy Covariance Latent Heat Flux: Inter-Comparison of Four Machine  
350 Learning Model Predictions and Uncertainties in Forest Ecosystem, *J. Remote Sens.*, 13, 4976.  
351 <https://doi.org/10.3390/rs13244976>, 2021.

352 Khan, M.S.; Liaqat, U.W.; Baik, J.; Choi, M.: Stand-alone uncertainty characterization of GLEAM, GLDAS and MOD16  
353 evapotranspiration products using an extended triple collocation approach, *J. Agric. For. Meteorol.*, 252, 256–268,  
354 <https://doi.org/10.1016/j.agrformet.2018.01.022>, 2018.

355 Kim, Y.; Johnson, M.S.; Knox, S.H.; Black, T.A.; Dalmagro, H.J.; Kang, M.; Kim, J.; Baldocchi, D.: Gap-filling approaches  
356 for eddy covariance methane fluxes: A comparison of three machine learning algorithms and a traditional method with  
357 principal component analysis, *J. Glob. Chang. Biol.*, 26, 1499–1518, <https://doi.org/10.1111/gcb.14845>, 2020.

358 Kunwor, S., Starr, G., Loescher, H. W., and Staudhammer, C. L.: Preserving the variance in imputed eddy covariance  
359 measurements: Alternative methods for defensible gap filling, *J. Agr. Forest Meteorol.*, 232, 635–649,  
360 <https://doi.org/10.1016/j.agrformet.2016.10.018>, 2017.

361 Li, X., Z. Gao, Y. Li, and B. Tong.: Comparison of sensible heat fluxes measured by a large aperture scintillometer and eddy  
362 covariance system over a heterogeneous farmland in East China, *J. Atmosphere.*, 8, 101, [https://doi.org/10.3390/](https://doi.org/10.3390/atmos8060101)  
363 [atmos8060101](https://doi.org/10.3390/atmos8060101), 2017.

364 Liu, J.; Zuo, Y.; Wang, N.; Yuan, F.; Zhu, X.; Zhang, L.; Zhang, J.; Sun, Y.; Guo, Z.; Guo, Y.; et al.: Comparative Analysis  
365 of Two Machine Learning Algorithms in Predicting Site-Level Net Ecosystem Exchange in Major Biomes, *J. Remote*  
366 *Sens.*, 13, 2242, <https://doi.org/10.3390/rs13122242>, 2021.

367 McCandless, T., Gagne, D. J., Kosović, B., Haupt, S. E., Yang, B., Becker, C., & Schreck, J. (2022). Machine Learning for  
368 Improving Surface-Layer-Flux Estimates. *Boundary-Layer Meteorology*, 185(2), 199-228.

369 Moffat, A. M., Papale, D., Reichstein, M., Hollinger, D. Y., Richardson, A. D., Barr, A. G., Beckstein, C., Braswell, B. H.,  
370 Churkin G., Desai, A. R., Falge, E., Gove, J. H., Heimann, M., Hui, D., Jarvis, A. J., Kattge, J., Noormets, A., and Stauch,  
371 V. J.: Comprehensive comparison of gap-filling techniques for eddy covariance net carbon fluxes, *J. Agr. Forest Meteorol.*,  
372 147, 209–232, <https://doi.org/10.1016/j.agrformet.2007.08.011>, 2007.

373 Moncrieff, J.; Clement, R.; Finnigan, J.; Meyers, T.: Averaging, Detrending, and Filtering of Eddy Covariance Time Series.  
374 In *Handbook of Micrometeorology: A Guide for Surface Flux Measurement and Analysis*, The Netherlands, pp., 7–31,  
375 [https://doi.org/10.1007/1-4020-2265-4\\_2](https://doi.org/10.1007/1-4020-2265-4_2), 2006.

376 Monin, A. S., & Obukhov, A. M. (1954). Basic laws of turbulent mixing in the surface layer of the atmosphere. *Contrib.*  
377 *Geophys. Inst. Acad. Sci. USSR*, 151(163), e187.

378 Nisa, Z.; Khan, M.S.; Govind, A.; Marchetti, M.; Lasserre, B.; Magliulo, E.; Manco, A.: Evaluation of SEBS, METRIC-  
379 EEFlux, and QWaterModel Actual Evapotranspiration for a Mediterranean Cropping System in Southern Italy, *J. Remote*  
380 *Sens.*, 13, 4976 18 of 19, <https://doi.org/10.3390/agronomy11020345>, 2021.

381 Papale, D.; Reichstein, M.; Aubinet, M.; Canfora, E.; Bernhofer, C.; Kutsch, W.; Longdoz, B.; Rambal, S.; Valentini, R.;  
382 Vesala, T.; et al.: Towards a standardized processing of Net Ecosystem Exchange measured with eddy covariance  
383 technique: Algorithms and uncertainty estimation, *J. Biogeosciences.*, 3, 571–583, <https://doi.org/10.5194/bg-3-571-2006>,  
384 2006.

385 Reichstein, M.; Falge, E.; Baldocchi, D.; Papale, D.; Aubinet, M.; Berbigier, P.; Bernhofer, C.; Buchmann, N.; Gilmanov, T.;  
386 Granier, A.; et al.: On the separation of net ecosystem exchange into assimilation and ecosystem respiration: Review and  
387 improved algorithm, *J. Glob. Change Biol.*, 11, 1424–1439, <https://doi.org/10.1111/j.1365-2486.2005.001002.x>, 2005.

388 Richard, A.; Fine, L.; Rozenstein, O.; Tanny, J.; Geist, M.; Pradalier, C.: Filling Gaps in Micro-Meteorological Data,  
389 Switzerland, [https://doi.org/10.1007/978-3-030-67670-4\\_7](https://doi.org/10.1007/978-3-030-67670-4_7), 2020.

390 Stauch, V.J.; Jarvis, A.J.: A semi-parametric gap-filling model for eddy covariance CO<sub>2</sub> flux time series data, *J. Glob. Chang.*  
391 *Biol.*, 12, 1707–1716, <https://doi.org/10.1111/j.1365-2486.2006.01227.x>, 2006.

392 Vitale, D., Bilancia, M., Papale, D.: A multiple imputation strategy for eddy covariance data, *J. Environ. Inform.*, 34, 68–87,  
393 <https://doi.org/10.3808/jei.201800391>, 2018.

394 Wang, L.; Wu, B.; Elnashar, A.; Zeng, H.; Zhu, W.; Yan, N.: Synthesizing a Regional Territorial Evapotranspiration Dataset  
395 for Northern China, *J. Remote Sens.*, 13, 1076, <https://doi.org/10.3390/rs13061076>, 2021.

396 Webb, E.K.; Pearman, G.I.; Leuning, R. Correction of flux measurements for density effects due to heat and water vapor  
397 Transfer, *Q. J. R. Meteorol. Soc.*, 106, 85–100, <https://doi.org/10.1002/qj.49710644707>, 1980.

398 Wilson, K.B.; Hanson, P.J.; Mulholland, P.J.; Baldocchi, D.D.; Wullschleger, S.D.: A comparison of methods for determining  
399 forest evapotranspiration and its components: Sap-flow, soil water budget, eddy covariance and catchment water balance,  
400 J. Agric. For. Meteorol., 106, 153–168, [https://doi.org/10.1016/S0168-1923\(00\)00199-4](https://doi.org/10.1016/S0168-1923(00)00199-4), 2001.

401 Wutzler, T., Lucas-Moffat, A., Migliavacca, M., Knauer, J., Sickel, K., Sigut, L., Reichstein, M.: Basic and extensible post-  
402 processing of eddy covariance flux data with REddyProc, J. Biogeosciences., 15 (16): 5015–5030,  
403 <https://doi.org/10.5194/bg-15-5015-2018>, 2018.

404 Yu, T.C.; Fang, S.Y.; Chiu, H.S.; Hu, K.S.; Tai, P.H.Y.; Shen, C.C.F.; Sheng, H.: Pin accessibility prediction and optimization  
405 with deep learning-based pin pattern recognition, J. IEEE Trans. Comput.-Aided Des. Integr. Circuits Syst., 40, 2345–  
406 2356, <https://doi.org/10.1145/3316781.3317882>, 2019.